Influence of the Excitation Wavelength on First Order Hyperpolarizabilities and Optimal Gap Tuning of Range Separated Hybrid Functionals

*Shyam Parshotam, Julianne M. Gibbs, and Alex Brown**

Department of Chemistry, University of Alberta, Edmonton, Alberta, T6G 2G2, Canada

*E-mail: alex.brown@ualberta.ca

Abstract

In this study, we compute the hyperpolarizability of the nitroaniline isomers, para-nitroaniline (pNA), ortho-nitroaniline (oNA), and meta-nitroaniline (mNA), by density functional theory (DFT), including with optimally tuned range separated hybrid (RSH) functionals. By utilizing the nitroanilines hyperpolarizability trend based on charge transfer (pNA>oNA>mNA), we can uncover how the excitation wavelength affects the prediction of the hyperpolarizabilities in both on and off resonant regimes, and optimal gap tuning of RSH functionals. In non-resonant regions, with reference to CCSD/aug-cc-pVDZ and experimental studies, we find that some computational approaches do not always reproduce the nitroanilines trend at specific excitation wavelengths. For example, RSH functionals require optimal gap tuning to reproduce the trend. In resonant regions, we find that the damped response theory predicts that the trend is maintained at the two-photon absorption, however, it breaks near the one photon pole. This suggests that the underlying charge transfer characteristics are undermined in the one-photon pole which in comparison to the two-state model suggests that this is due to the presence of other electronic states in some of the

isomers. Furthermore, we find that cases where optimal gap tuning is ineffective (pathological behavior) are dependent on the excitation wavelength.

Introduction

Devices and techniques utilizing second order nonlinear optical properties have found extensive applications in telecommunications and surface sensitive characterization techniques.[1–4] Central to these applications is the magnitude of the first molecular hyperpolarizability, β_{ijk}, which is directly related to the extent of charge transfer within a system. The magnitude of the molecular hyperpolarizability can be determined via experimental routes, such as electric field-induced second harmonic generation (EFISH) and hyper-Rayleigh-scattering (HRS) experiments.[5–7] In these experiments, light with an excitation or fundamental wavelength (λ_{ex}) interacts with a species to yield an output with half the wavelength ($\frac{\lambda_{ex}}{2}$). Complementary to experimental measurements, over the last three decades, extensive computational work involving the use of various theoretical methods to predict the hyperpolarizability has been achieved.[8–11] The bulk of these studies have been accomplished at off-resonant excitation wavelengths. While it is known that the hyperpolarizability can be resonantly enhanced at the one-photon pole ($\lambda_{ex} = \Delta E$) and the two-photon pole ($2\lambda_{ex} = \Delta E$), it is unclear how the underlying charge transfer characteristics of a system would behave in these resonance regimes.

A commonly used reference system in previous studies is the push-pull π-conjugated molecule, para-nitroaniline (pNA), which has been thoroughly investigated both experimentally and computationally.[5,12–21] Compared to meta (mNA) and ortho (oNA) nitroaniline isomers (Figure 1), it displays a remarkably larger hyperpolarizability as shown in both EFISH and HRS experiments at off resonant excitation wavelengths (λ_{ex} =1064 nm and 1907 nm), which

consequently led to determining the hyperpolarizability trend of pNA>oNA>mNA.[5,22–25] Early theoretical studies based on a two-state model attributed the trend to the intramolecular charge transfer between the donor (-NH_2) and acceptor (-NO_2) groups in the nitroaniline isomers, which has led to computational and experimental investigations into more push-pull type π-conjugated systems.[23,25–27]

The use of computational methods in the evaluation of both on and off resonant hyperpolarizabilities face challenges in reproducing the experimental measurements. Early computations involving the use of Hartree-Fock and semi-empirical methods were found to severely underestimate the hyperpolarizabilities relative to correlated methods based on coupled cluster and second-order Møller-Plesset perturbation theory (MP2).[31–34] Although the use of electron correlated methods has a profound effect on the accuracy of the hyperpolarizability, their practicality, computational cost, and convergence behavior, limit the widespread use of these methods in computations of hyperpolarizabilities.[35]

On the other hand, the use of density functional theory (DFT) provides an alternative route at a fraction of the computational cost. However, these methods are also susceptible to challenges in accurately predicting hyperpolarizability values, stemming from the choice of the exchange-correlation (XC) functional.[26,36] Hybrids and generalized gradient approximation (GGA) functionals poorly describe charge transfer excitations due to the wrong asymptotic behavior in the Coulomb operator.[37,38] To overcome this weakness, the concept of the range-separated hybrid functionals (RSH) was developed, where the Coulomb operator is partitioned into short- and long-range parts, using a standard error function.[39–42] Based on this formulation, a new variable called the range separation parameter, ω (or μ), is needed, which controls the switching between short-range and long-range behavior. An overall improvement is observed in the prediction of nonlinear

optical properties of systems with RSH functionals relative to traditional GGA functionals, however the tendencies to over or underestimate the properties relative to experimental studies still persists.[43–46] An approach to improve the description of hyperpolarizabilities involves the optimization of the range separation parameter by a process known as nonempirical optimal gap tuning, which entails the enforcement of the molecule and its anion to obey Koopman's theorem.[47–51] However, due to the sensitivity to the environment, this approach has provided predictions with variable success relative to the experimental values and high-level ab initio computations.[12,45,52–54]

As such in this study, we utilize the known nitroaniline isomers' hyperpolarizability trend (pNA>oNA>mNA) as a means of qualitatively assessing the role of the excitation wavelength on the computation of hyperpolarizabilities. By computing the hyperpolarizabilities at different excitation wavelengths in addition to the static limit, we observe that the nitroanilines trend is not always maintained in on and off resonant conditions. For example, in the off-resonant and the two-photon absorption region (500-700 nm) the trend is maintained, however below this region and in the one photon region (250-350 nm) it is no longer maintained. Comparison to the damped two model suggests the resonance enhancement and possible presence of other states could dominate the charge transfer characteristics. Furthermore, we find that the previously identified pathological behavior associated with optimal gap tuning is wavelength dependent.

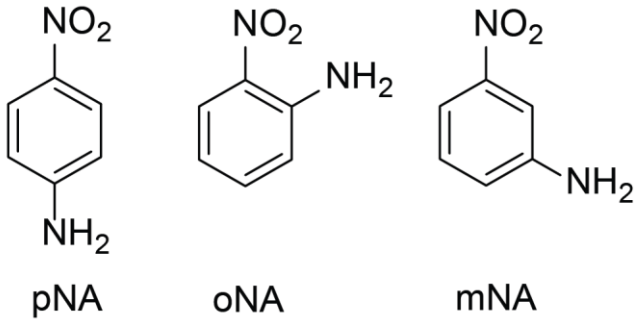

Figure 1: Structures of the nitroaniline isomers: para-nitroaniline (pNA), ortho-nitroaniline (oNA), and meta-nitroaniline (mNA).

Computational Details

Density functional theory (DFT) computations on the nitroaniline isomers (Figure 1) were carried out using the Gaussian 16 suite of programs,[55] while coupled cluster and time dependent density functional theory (TDDFT) with damped response theory computations were done in Dalton 16.[56] The geometries of pNA, oNA, and mNA were optimized with CAM-B3LYP/6-31+G(d,p) using default convergence parameters.[57–63] The optimized geometries for each of the molecules are provided in the supplementary material.

First-order hyperpolarizabilities computed with DFT utilized the following functionals: B3LYP,[64] CAM-B3LYP,[57] ωB97XD,[65] ωB97,[66] and LC-BLYP[39] with the 6-311+G(d,p) basis set in both the gas and solvent phases. Additional TDDFT computations were done with the same basis set.[67] All solvent effects in DFT computations were accounted for with the polarizable continuum model (IEF-PCM).[68] Additional gas phase computations were done with second-order approximate coupled cluster (CC2), coupled cluster singles (CCS), and coupled cluster with singles and doubles (CCSD), with the use of the frozen core approximation and the aug-cc-pVDZ basis set.[56,69,70] The range-separated hybrid functionals (RSH) were non-empirically tuned by setting the values of the range separation parameter (ω) with the internal options (IOps) for the

anion, cation, and neutral species of the molecule in the gas phase.[47–49] Tuning was accomplished by minimizing the absolute difference (J^2) via

$$J^2(\omega) = [\epsilon_{HOMO}(N) + IP(N)]^2 + [\epsilon_{HOMO}(N+1) + IP(N+1)]^2 \,, \quad (1)$$

where IP refers to the ionization potential of the species (neutral = N electrons and anion = N+1 electrons) and ϵ_{HOMO} is the energy of the highest occupied molecular orbital of the corresponding species. To take solvation into account in optimal tuning studies, we utilize one of the approaches suggested by Kronik and Kümmel,[71] whereby optimal gap tuning is achieved in the gas phase and subsequent PCM is added using the ω value obtained in the gas phase. To avoid confusion in differentiating the range separation parameter, ω, and excitation energy (wavelength), we label the latter as λ_{ex}.

Hyperpolarizabilities are presented in the 'T' convention, which is based on the Taylor series expansion of the induced dipole moment, μ,

$$\mu(E) = \mu_i^o + \alpha_{ij}E + \beta_{ijk}EE + \gamma_{ijkl}EEE \,. \quad (2)$$

In Eq. 2.2, μ_i^o represents the permanent dipole moment, without the presence of the field E, α_{ij} is the polarizability, β_{ijk} is the first hyperpolarizability, and γ_{ijkl} is the second hyperpolarizability. The subscripts '*ijk*' and *'ijkl'* indicate that the hyperpolarizabilities are tensors with components defined in the molecular principal axis frame. The reported values, in atomic units (au), are the vector components of the hyperpolarizability which are parallel to the permanent dipole moment, $\beta_{||}$. This value is related to tensor components by

$$\beta_{||} = \frac{1}{5}\sum_i(\beta_{zii} + \beta_{izi} + \beta_{iiz}) \,. \quad (3)$$

For computations where the coordinate system does not align with the dipole moment, the value is given by[4]

$$\beta_{||} = \frac{1}{5}(\beta_x^2 + \beta_y^2 + \beta_z^2)^{1/2} \,, \quad (4)$$

where the components β_j are

$$\beta_j = \frac{1}{5}\sum_i \left(\beta_{jii} + \beta_{iji} + \beta_{iij}\right) . \quad (5)$$

For excitation energies near an electronic resonance, it has been shown that the hyperpolarizabilities should be determined through a damped two-state model (TSM). [21,28,72–76] In this model, the hyperpolarizability is given by

$$\beta_{ijk}(-2\omega;\omega_1,\omega_2) = P\ \sum_{m\neq 0}\sum_{n\neq 0}\left\{\frac{\langle 0|\mu_i|m\rangle\langle m|\overline{\mu_j}|n\rangle\langle n|\mu_k|0\rangle}{(\omega_{m0}+2\omega-i\gamma)(\omega_{n0}-\omega_1-i\gamma)} + \frac{\langle 0|\mu_k|m\rangle\langle m|\overline{\mu_j}|n\rangle\langle n|\mu_k|0\rangle}{(\omega_{m0}+\omega_2+i\gamma)(\omega_{n0}-2\omega+i\gamma)} + \frac{\langle 0|\mu_k|m\rangle\langle m|\overline{\mu_j}|n\rangle\langle n|\mu_j|0\rangle}{(\omega_{m0}+\omega_2+i\gamma)(\omega_{n0}-\omega_1-i\gamma)}\right\} . \quad (6)$$

where the term $\langle m|\bar{\mu}|n\rangle = \langle m|\mu|n\rangle - \langle 0|\mu|0\rangle$. In Eq. 6, *P* is a permutation operator taking all the combinations into account, ω_{m0} is the excitation energy between the ground and *m*th state, $\langle n|\mu_k|0\rangle$ is the transition dipole moment between the ground and *n*th excited state, and γ is the damping parameter.

In the damped response theory, we compute the isotropic average hyperpolarizability based on the previous work,[21]

$$\bar{\beta} = \frac{1}{5}\sum_i(\beta_{zii} + 2\beta_{izi}) . \quad (7)$$

The inclusion of the relaxation results in complex hyperpolarizability values. Therefore, we present the absolute values. To facilitate a comparison between the computed and experimental values, experimental calibration and conversion factors were considered.[14,77] Details are provided in the supplementary material.

Results and Discussion

We begin the discussion by commenting on the influence of optimal gap tuning on the value of the range separation parameter (ω) of the range separated hybrid (RSH) functionals. The

values were optimized in the gas phase, with $\pm$ 0.02 Bohr^{-1} accuracy, as shown in the plots of the absolute errors (J^2) versus ω in the supplementary material (Figure S1). Relative to the default values of the range separation parameter, optimal gap tuning significantly affects ωB97XD (ω = 0.33 to 0.20) as compared to LC-BLYP and ωB97 (ω = 0.33 to 0.28) for all the nitroaniline isomers. The values of ω for pNA closely match those predicted by the previous work done with different basis sets.[12,78]

With the tuned RSH functionals in hand, the gas phase hyperpolarizabilities at the static limit ($\lambda_{ex} = \infty$) and dynamic (λ_{ex}= 1064 nm) were computed, along with computations with B3LYP, CAM-B3LYP, CCS, CC2, and CCSD as presented in Table 1. Assessing the dynamic hyperpolarizabilities ($\beta_{||}^{1064nm}$) with the experimental hyperpolarizability trend (pNA > oNA > mNA), we find that the RSH functionals can reproduce the dynamic hyperpolarizability trend without optimal gap tuning being required. When assessing the hyperpolarizability trend predicted by the other methods, we find that B3LYP, CCS, and CAS/DZP,[20] are unable to reproduce the experimental trend. Although B3LYP provides a good approximation of pNA relative to the CCSD computation, it performs poorly for the other isomers. The tendency of B3LYP to predict well the hyperpolarizability of pNA, but under or over-estimate for other systems is well documented.[18] The failure of CCS is not surprising too, as previous studies done on pNA in the gas phase indicate that it will underestimate the static hyperpolarizabilities relative to CCSD computations, whereas CC2 will do the opposite.[18,35] As we show here, these behaviors associated with CCS and CC2 extend to the dynamic hyperpolarizabilities (λ_{ex} = 1064 nm) and the other nitroaniline isomers studied here.

Table 1: Gas phase static and dynamic hyperpolarizabilities (in au) of the nitroaniline isomers computed with DFT functionals and wave function theory-based methods with 6-311+G(d,p) and

aug-cc-pVDZ basis sets, respectively. Optimally tuned RSH functionals are distinguished by an asterisk (*).

Method	**pNA**		**oNA**		**mNA**	
	$\beta_{\|\|}^{Static}$	$\beta_{\|\|}^{1064nm}$	$\beta_{\|\|}^{Static}$	$\beta_{\|\|}^{1064nm}$	$\beta_{\|\|}^{Static}$	$\beta_{\|\|}^{1064nm}$
B3LYP	908	1646	252	604	342	635
CAM-B3LYP	791	1274	271	543	285	437
ωB97XD	803	1271	279	526	298	449
ωB97XD*	789	1230	280	518	291	432
ωB97	725	1082	277	473	257	358
ωB97*	778	1230	280	539	282	419
LC-BLYP	739	1095	288	482	261	360
LC-BLYP*	827	1330	297	588	302	457
HF	518	710	197	287	168	222
CC2	1255	2025	325	586	359	533
CCS	581	779	185	247	204	272
CCSD	987	1495	291	476	311	438
CAS[a]	805	1097	231	267	241	321
PM3[b]	729	NR	116	NR	231	NR

[a] *Static and dynamic hyperpolarizabilities ($\beta_{||}$) based on the use of complete active space and double zeta valence (DZV) basis set with polarization functions on all atoms.*[20] *$\beta_{||}$ for the isomers are calculated using the individual tensor components provided and equation 4.*

[b] *Static hyperpolarizabilities from Ref.* 79. *Dynamic hyperpolarizabilities not reported (NR).*

On the other hand, assessing the static hyperpolarizabilities, ($\beta_{||}^{Static}$), of the nitroaniline isomers, we find that CCSD/aug-cc-pVDZ computations indicate that the trend of the isomers does not follow the one predicted by experiments (pNA > oNA > mNA) instead the hyperpolarizability of mNA is greater than oNA where the trend becomes pNA > mNA > oNA. As a result, CC2, CCS, B3LYP, CAM-B3LYP, the previous CAS/DZP, PM3, and B3LYP/aug-cc-pVDZ computations done on the isomers follow this trend in the hyperpolarizabilities at the static limit.[15,20,79] The change in the hyperpolarizability trend suggests that the excitation wavelength

plays a role in the computation of hyperpolarizabilities in off resonant conditions. This is surprising as it suggests that the underlying charge transfer characteristics of the nitroanilines do not always persist.

The effect of optimal gap tuning becomes apparent at the static limit too, where the untuned RSH functionals ωB97 and LC-BLYP do not follow the static hyperpolarizability trend being predicted by the CCSD/aug-cc-pVDZ computations. However, after tuning the range separation parameter as described before, the functionals follow the trend predicted by the CCSD/aug-cc-pVDZ computation. We do note that tuning has a minimal influence on oNA at the static limit as compared to at 1064 nm, where for example ωB97XD changes by 1 au at the static limit compared to 7 au at 1064 nm. Nevertheless, this shows that optimal gap tuning is necessary to improve the description of static hyperpolarizabilities relative to CCSD/aug-cc-pVDZ computations.

To determine whether these changes in the hyperpolarizability trend persist in the presence of a solvent, we compare the computed hyperpolarizability trend to experimental studies determined at two excitation wavelengths ($\beta_{||}^{1064nm}$ & $\beta_{||}^{1907nm}$) which are in the presence of different media (Table 2).[5,23,24] The significant shift in the experimental hyperpolarizabilities at the different excitation wavelengths cannot be solely attributed to the change in the excitation wavelength. Previous work has highlighted the vibrational contributions, solvent effects and systematic errors associated with the experimental measurements can lead to different hyperpolarizabilities.[14,22,72,77,80] Nonetheless, all experiments show that the hyperpolarizability trend (pNA>oNA>mNA) persists at these off-resonant frequencies.

Table 2: Dynamic hyperpolarizabilities (in au) with λ_{ex}= 1064 nm and 1907 nm of the nitroaniline isomers computed with the default DFT functionals and optimally tuned functionals (distinguished by an asterisk (*)).

	pNA		**oNA**		**mNA**	
Method	$\beta_{\|\|}^{1064nm}$	$\beta_{\|\|}^{1907nm}$	$\beta_{\|\|}^{1064nm}$	$\beta_{\|\|}^{1907nm}$	$\beta_{\|\|}^{1064nm}$	$\beta_{\|\|}^{1907nm}$
Ref. 5[a]	6112	-	1333	-	874	-
Ref. 23[a]	5750	-	1417	-	833	-
Ref. 24[b]	-	2162	-	521	-	396
B3LYP	4070	2131	1310	600	1959	801
CAM-B3LYP	3160	1785	1150	610	1035	616
ωB97XD	2919	1683	1106	591	971	592
ωB97XD*	2830	1645	1089	590	925	574
ωB97	2450	1476	991	568	727	487
ωB97*	2814	1629	1112	600	890	558
LC-BLYP	2508	1503	1018	586	731	490
LC-BLYP*	3111	1751	1220	639	986	601
HF	1594	1023	617	383	499	346

[a] *Experimental values of Levine and Bethea*[5] *as well as Oudar and Chemla*[23] *which measured pNA in methanol, and oNA/ mNA in acetone at* λ_{ex} *= 1064 nm.*

[b] *Experimental values derived from Cheng et al.*[24] *where pNA was measured in acetone whereas mNA and oNA were measured in 1,4-dioxane at* λ_{ex} *= 1907 nm.*

At λ_{ex} = 1064 nm, several similarities to the gas phase computations of $\beta_{||}^{1064nm}$ can be found, where the traditional GGA functional B3LYP is the only functional unable to reproduce this trend as it overestimates the hyperpolarizability of mNA. Likewise, the need for optimal gap tuning is unnecessary at this excitation wavelength. On the other hand, at λ_{ex} = 1907 nm, B3LYP, CAM-B3LYP, and ωB97XD fail to reproduce the experimental trend. Although it is not surprising for B3LYP to fail to reproduce the experimental trend, it is surprising for CAM-B3LYP and ωB97XD as they can do so at 1064 nm. Indeed, similar to the gas phase static hyperpolarizabilities, optimal gap tuning corrects the behavior of ωB97XD. Furthermore, tuning

ωB97XD has a minimal effect on oNA at 1907 nm where the hyperpolarizability changes by 1 au as compared to a change of 17 au observed at 1064 nm.

The difference in the behavior of functionals at different excitation wavelengths indicates the role the excitation wavelength plays in both the prediction of the hyperpolarizabilities and optimal gap tuning. To further investigate the first connection, the hyperpolarizabilities were computed at excitation wavelengths utilized by Ref.13 in their experimental EFISH study conducted on pNA in 1,4 dioxane (experimental excitation wavelength dependent hyperpolarizabilities of mNA and oNA have not been determined). Adopting their excitation wavelengths, we evaluate the performance of the functionals with solvent effects of 1,4 dioxane (PCM) being considered. Figure 2(a) compares the $\beta_{||}$ of pNA computed at the wavelengths employed in the EFISH experiment. All the RSH functionals can reproduce the increment seen in the experimental hyperpolarizability of pNA with varying degrees of accuracy relative to the experiment. CAM-B3LYP and ωB97XD provide a closer approximation to the experimental values than ωB97 and LC-BLYP. The accuracy relative to the experiment is dependent on the excitation wavelength as the error significantly increases at shorter excitation wavelengths (higher energies).

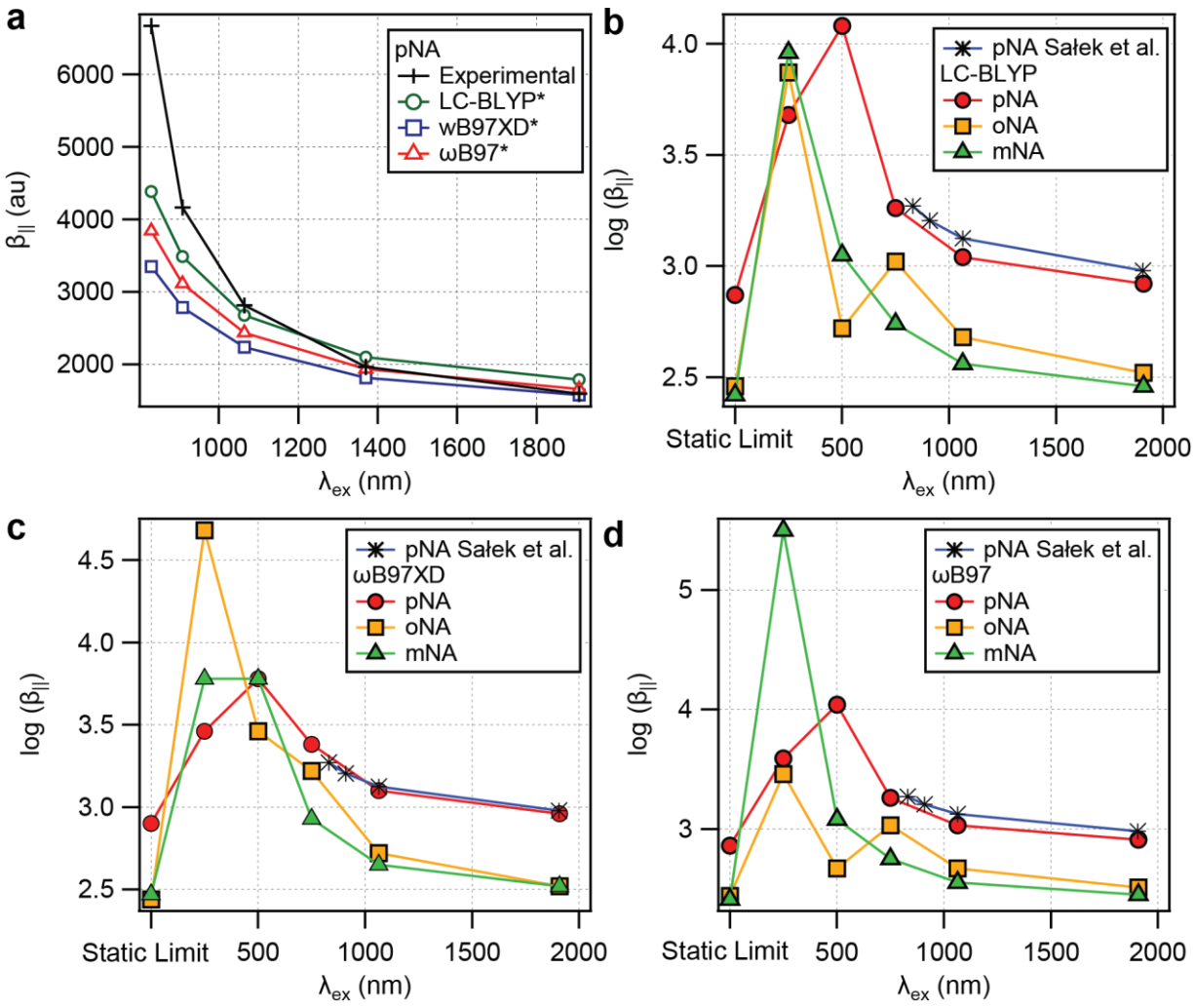

Figure 2: (a) Variation of the $\beta_{||}$ of pNA as a function of the excitation wavelength for all RSH functionals in comparison to experimental values.[13] Computations were done in 1,4 dioxane. Gas phase (b-d) log ($\beta_{||}$) of all isomers in a broader wavelength range from 1907 nm to the static limit. Additional gas phase CCSD/aug-cc-pVDZ computations on pNA from Sałek et al.[18] are presented too.

To obtain a qualitative picture of the excitation wavelength dependence, the gas phase hyperpolarizabilities were computed with RSH functionals over a wider excitation wavelength window (Figure 2(b-d)). Additional previous CCSD/aug-cc-pVDZ computations done by Sałek et al. are also included.[18] The hyperpolarizabilities of all the nitroaniline isomers significantly increase as the wavelength is lowered from 1907 nm to 750 nm. From 830 - 1907 nm, notably, the ωB97XD results provide a closer approximation to the previous CCSD/aug-cc-pVDZ values of

pNA than ωB97 and LC-BLYP. In this region, all the default RSH functionals can reproduce the experimental hyperpolarizability trend. However, between 500 nm and the static limit, there is no consistency between the RSH functionals, as each gives different nitroaniline hyperpolarizability trends. We tentatively assign this enhancement of the hyperpolarizabilities to the presence of electronic resonances for all isomers. Indeed, TDDFT computations summarized in Table S2 confirm that the electronic resonances for the isomers lie between 250 - 350 nm. Moreover, the presence of the electronic resonance can explain the different nitroaniline trend predicted by the gas phase CCSD/aug-cc-pVDZ computations at the static limit. This change in the hyperpolarizability trend highlights the effect an electronic resonance can have on the computation of the hyperpolarizabilities.

We can shed light on the influence of the electronic resonances by evaluating the hyperpolarizability in greater resolution by using the damped two-state model (TSM) in the near and on resonance regions. The damping parameter is set to 500 cm^{-1} based on previous work on pNA.[21] As shown in Figure 3(a), the damped two-state model predicts that all isomers shows two distinct resonant centers or pole positions when the excitation energy is in close proximity to a resonant contribution. The first region between 250-350 nm (labelled '(i)') is the one-photon resonance regime whereby the excitation energy is at resonance, while the second region between 500 – 700 nm (labelled '(ii)') is the two-photon resonance regime whereby the second harmonic energy overlaps with the resonant energy.[28,81]For pNA, these regions are in agreement with previous experimental and computational work.[82,83] We find that for both one and two photon resonance, and the region between them, the nitroanilines hyperpolarizability trend is reproduced by the damped two-state model suggesting that the underlying donor-acceptor charge transfer characteristics significantly contribute to the hyperpolarizabilities.[23]

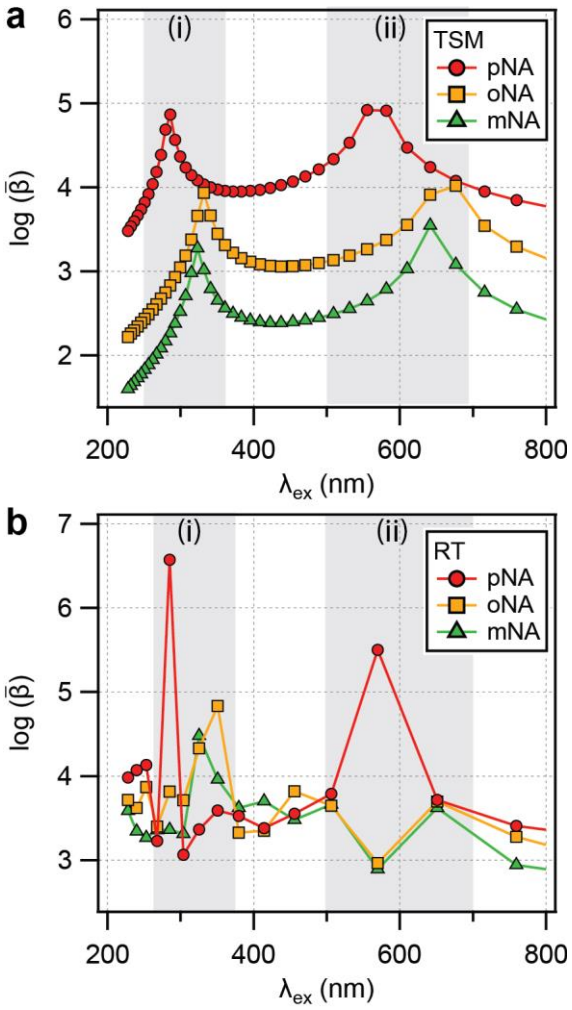

Figure 3: Hyperpolarizabilities determined using the (a) damped two-state model (TSM) and (b) damped response theory (RT). The value of the relaxation parameter (γ) is set to 500 cm^{-1} for both approaches. Parameters utilized to compute the hyperpolarizabilities of the TSM are presented in Table S3 in the supporting information. All computations are done with CAM-B3LYP/6-311+G(d,p) in the gas phase.

In Figure 3(b), we show the hyperpolarizabilities computed with damped response theory (RT). Similar to the TSM, the damping parameter (γ) is set to 500 cm^{-1}. In the two-photon resonance region (ii), we find that the hyperpolarizability trend is maintained. However, in two areas below this region (< 500 nm) the hyperpolarizability trend is not always maintained. Firstly, in the region between the one and two photon resonances, the trend is also broken, likely due to

the damped two-state model (even with damping) not accounting for the additional electronic or vibronic states that are able to contribute to the hyperpolarizabilities in these regions.[72,84,85]

Secondly, in the one photon resonance region, a direct comparison of RT to the TSM (Figure S3), shows that while good agreement can be found in the prediction of one-photon pole positions for pNA and mNA, this is not the case for oNA. Such a shift in the pole positions between the RT and TSM has been identified for LiH.[76] This was linked to the prediction of an additional false pole by RT due to the shortcomings of the adiabatic approximation. Indeed, the variations in the occurrence of the shifts in the isomers suggest the presence of additional poles is highly system dependent and thus the comparison to the damped two state model can serve as a good reference.

Next, we investigate the role the excitation wavelength plays in optimal gap tuning. The hyperpolarizabilities were computed over the experimental excitation wavelength range (830-1907 nm) with the tuned RSH functionals (Figure S2(a)). In comparison to the experimental values, tuning the RSH functionals over this wavelength range has a variable effect on the accuracy of the predicted hyperpolarizabilities in 1,4 dioxane.[13] The accuracy improves for LC-BLYP and ωB97 at 803, 909, and 1064 nm, however, reduces at 1907nm. In comparison to the gas phase CCSD/aug-cc-pVDZ computations done by Sałek et al.[18] on pNA, optimal gap tuning improves the prediction of the hyperpolarizabilities by ωB97 and LC-BLYP (Figure S2(b-d)). On the other hand, the opposite behavior takes place for ωB97XD, where the prediction improves at 1907 nm while becoming worse at the lower excitation wavelengths. For all the RSH functionals at the static limit and 1907 nm, tuning the functionals has a minimal effect on the hyperpolarizabilities of oNA.

The small change due to optimal gap tuning is interesting to note as this indicates that optimal gap tuning has a minimal influence on the hyperpolarizabilities of oNA. To explore these changes in oNA, we utilized the diagnostic test proposed by Scuseria and coworkers.[12] In this test, optimal gap tuning is effective when $\beta_{||}$ decays as the value of the range separation parameter (ω) increases. However, when this behavior is not followed, optimal gap tuning becomes less likely to improve the computed hyperpolarizabilities relative to experimental measurements. This approach was developed on pyrrole derivatives which displayed an increase in the $\beta_{||}$ values followed by a decrease as the value of ω was increased. Optimal gap tuning was found to have a minimal influence on the hyperpolarizabilities of these derivatives in comparison to that of pNA. Indeed, such behavior has been observed in other charge transfer systems.[54]

Based on these observations, we present the plots of the $\beta_{||}$ of oNA as a function of ω at different excitation wavelengths in Figure 4. At the static limit and 1907 nm, all RSH functionals show that the $\beta_{||}$ rises initially followed by a decline as the value of ω increases (Figure 4 (a & c)). This behavior is similar to that found with the pyrrole derivatives and suggests that oNA represents a pathological case at the static limit and 1907 nm.[12] However, as shown in Figure 3(b), at 1064 nm a typical decay curve is observed indicating that the molecule is not the only contributing factor to this pathological behavior, but the choice of the excitation wavelength can also contribute and results in optimal gap tuning having a minimal effect on the hyperpolarizabilities. We do note that pNA and mNA exhibit typical behavior as the $\beta_{||}$ decays as ω increases for all the excitation wavelengths (Figure S3). Furthermore, the behavior of all the nitroaniline isomers observed in the gas phase extends to computations done in the solvent phase (1,4 dioxane) as well (Figure S5). Hence, setting the correct excitation wavelength is an important parameter when gauging the efficacy of optimal gap tuning in the prediction of hyperpolarizabilities.

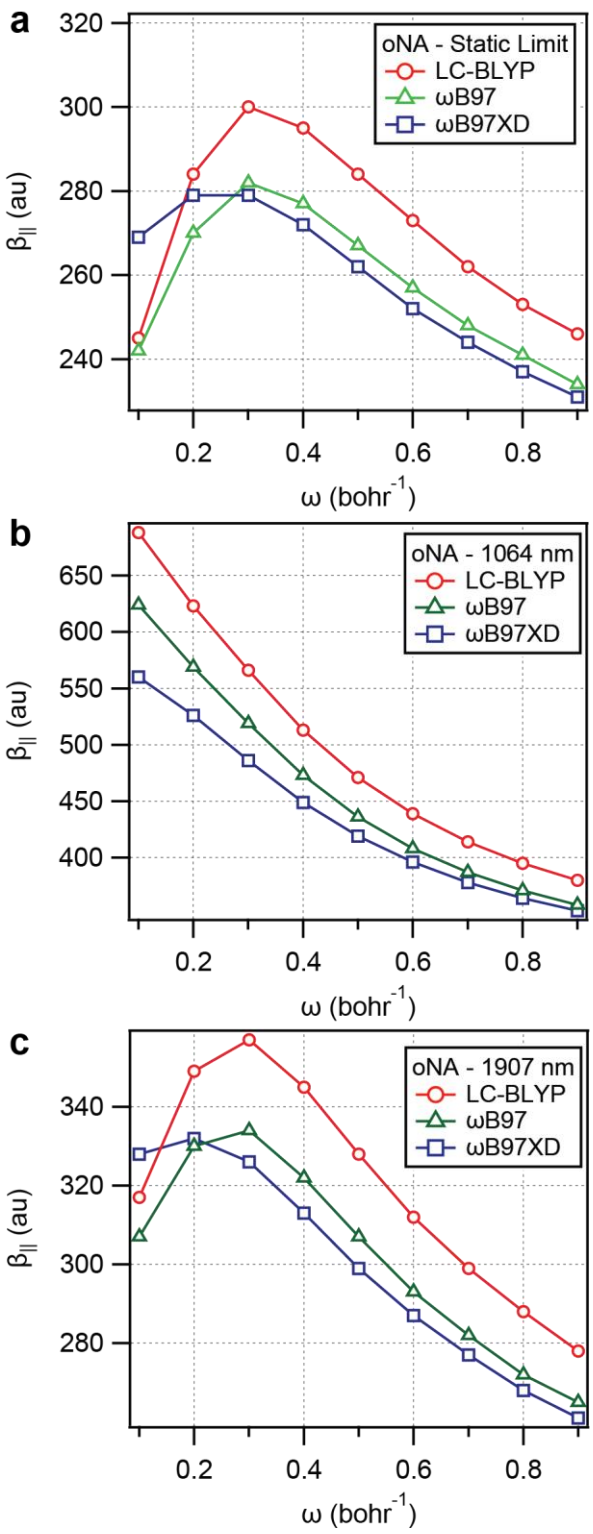

Figure 4: Variation of the hyperpolarizabilities ($\beta_{||}$) of oNA with respect to the range separation parameter (ω) for RSH functionals at (a) the static limit (b) 1064 nm, and (c) 1907 nm in the gas phase. All computations used the 6-311+G(d,p) basis set.

Conclusions

In conclusion, the hyperpolarizabilities of para, ortho, and meta-nitroaniline were evaluated using DFT, including with optimally tuned range separated functionals, and coupled cluster calculations utilizing the charge transfer based hyperpolarizability trend (pNA > oNA > mNA) as a qualitative measure of accuracy. The excitation wavelength plays a pivotal role in the prediction of the hyperpolarizability trend as it is not always maintained, for example CCSD/aug-cc-pVDZ computations at the static limit. Monitoring the hyperpolarizabilities over a wider excitation wavelength range with damped response theory indicates near the one-photon resonance region the trend is broken. Comparison to the damped two-state model reveals that the underlying charge transfer characteristics of the isomers are compromised by the presence of additional states or false poles in the one photon resonance region. The role of the excitation wavelength is also apparent in the optimal gap tuning process, where oNA exhibits pathological behavior which makes optimal gap tuning ineffective at 1907 nm and the static limit, but it reverts to the typical behavior at 1064 nm. These findings highlight that the excitation wavelength is an important factor to consider in both gas phase and solvent phase computations of hyperpolarizabilities and optimal gap tuning of RSH functionals.

Acknowledgments

AB and JMG thank the Natural Sciences and Engineering Research Council of Canada for financial support (Discovery Grants to both). Part of the research was carried out on the resources provided by WestGrid (www.westgrid.ca) and Digital Research Alliance of Canada (www.alliancecan.ca).

Supplementary Material

Plots of the absolute differences (J^2) against the range separation parameter used to determine the optimized ω values, previous experimental studies of hyperpolarizabilities were done on nitroaniline isomers, variation of the hyperpolarizability from the static limit to 2000 nm for the tuned RSH functionals, results from TDDFT computations, comparison of the damped response theory to the damped two state model, variation of the hyperpolarizabilities of pNA and mNA with respect to the range separation parameter for RSH functionals at the static limit, 1064 nm, and 1907 nm in the vacuum; and coordinates of the computed ground state geometries of all the nitroaniline isomers.

References

(1) *Non-Linear Optical Properties of Matter: From Molecules to Condensed Phases*; Papadopoulos, M. G., Sadlej, A. J., Leszczynski, J., Eds.; Challenges and advances in computational chemistry and physics; Springer: Dordrecht, 2006.

(2) *Nonlinear Optical Effects and Materials*; Günter, P., Ed.; Springer Series in Optical Sciences; Springer Berlin Heidelberg: Berlin, Heidelberg, 2000; Vol. 72. https://doi.org/10.1007/978-3-540-49713-4.

(3) Marder, S. R. Organic Nonlinear Optical Materials: Where We Have Been and Where We Are Going. *Chem. Commun.* **2006**, No. 2, 131–134. https://doi.org/10.1039/B512646K.

(4) Kurtz, H. A.; Dudis, D. S. Quantum Mechanical Methods for Predicting Nonlinear Optical Properties. In *Reviews in Computational Chemistry*; Lipkowitz, K. B., Boyd, D. B., Eds.; John Wiley & Sons, Inc.: Hoboken, NJ, USA, 2007; pp 241–279. https://doi.org/10.1002/9780470125892.ch5.

(5) Levine, B. F.; Bethea, C. G. Molecular Hyperpolarizabilities Determined from Conjugated and Nonconjugated Organic Liquids. *Appl. Phys. Lett.* **1974**, *24* (9), 445–447. https://doi.org/10.1063/1.1655254.

(6) Clays, K.; Persoons, A. Hyper-Rayleigh Scattering in Solution with Tunable Femtosecond Continuous-wave Laser Source. *Rev. Sci. Instrum.* **1994**, *65* (7), 2190–2194. https://doi.org/10.1063/1.1144725.

(7) Clays, K.; Persoons, A. Hyper-Rayleigh Scattering in Solution. *Phys. Rev. Lett.* **1991**, *66* (23), 2980–2983. https://doi.org/10.1103/PhysRevLett.66.2980.

(8) Shelton, D. P.; Rice, J. E. Measurements and Calculations of the Hyperpolarizabilities of Atoms and Small Molecules in the Gas Phase. *Chem. Rev.* **1994**, *94* (1), 3–29. https://doi.org/10.1021/cr00025a001.

(9) Champagne, B.; Perpète, E. A.; van Gisbergen, S. J. A.; Baerends, E.-J.; Snijders, J. G.; Soubra-Ghaoui, C.; Robins, K. A.; Kirtman, B. Assessment of Conventional Density Functional Schemes for Computing the Polarizabilities and Hyperpolarizabilities of

Conjugated Oligomers: An *Ab Initio* Investigation of Polyacetylene Chains. *J. Chem. Phys.* **1998**, *109* (23), 10489–10498. https://doi.org/10.1063/1.477731.
(10) Lescos, L.; Sitkiewicz, S. P.; Beaujean, P.; Blanchard-Desce, M.; Champagne, B.; Matito, E.; Castet, F. Performance of DFT Functionals for Calculating the Second-Order Nonlinear Optical Properties of Dipolar Merocyanines. *Phys. Chem. Chem. Phys.* **2020**, *22* (29), 16579–16594. https://doi.org/10.1039/D0CP02992K.
(11) de Wergifosse, M.; Grimme, S. Perspective on Simplified Quantum Chemistry Methods for Excited States and Response Properties. *J. Phys. Chem. A* **2021**, *125* (18), 3841–3851. https://doi.org/10.1021/acs.jpca.1c02362.
(12) Garza, A. J.; Osman, O. I.; Asiri, A. M.; Scuseria, G. E. Can Gap Tuning Schemes of Long-Range Corrected Hybrid Functionals Improve the Description of Hyperpolarizabilities? *J. Phys. Chem. B* **2015**, *119* (3), 1202–1212. https://doi.org/10.1021/jp507226v.
(13) Teng, C. C.; Garito, A. F. Dispersion of the Nonlinear Second-Order Optical Susceptibility of Organic Systems. *Phys. Rev. B* **1983**, *28* (12), 6766–6773. https://doi.org/10.1103/PhysRevB.28.6766.
(14) Reis, H. Problems in the Comparison of Theoretical and Experimental Hyperpolarizabilities Revisited. *J. Chem. Phys.* **2006**, *125* (1), 014506. https://doi.org/10.1063/1.2211611.
(15) Alam, M. M.; Beerepoot, M. T. P.; Ruud, K. A Generalized Few-State Model for the First Hyperpolarizability. *J. Chem. Phys.* **2020**, *152* (24), 244106. https://doi.org/10.1063/5.0010231.
(16) Paley, M. S.; Harris, J. M.; Looser, H.; Baumert, J. C.; Bjorklund, G. C.; Jundt, D.; Twieg, R. J. A Solvatochromic Method for Determining Second-Order Polarizabilities of Organic Molecules. *J. Org. Chem.* **1989**, *54* (16), 3774–3778. https://doi.org/10.1021/jo00277a007.
(17) Sim, F.; Chin, S.; Dupuis, M.; Rice, J. E. Electron Correlation Effects in Hyperpolarizabilities of P-Nitroaniline. *J. Phys. Chem.* **1993**, *97* (6), 1158–1163. https://doi.org/10.1021/j100108a010.
(18) Sałek, P.; Helgaker, T.; Vahtras, O.; Ågren, H.; Jonsson ⊥, D.; Gauss, J. A Comparison of Density-Functional-Theory and Coupled-Cluster Frequency-Dependent Polarizabilities and Hyperpolarizabilities. *Mol. Phys.* **2005**, *103* (2–3), 439–450. https://doi.org/10.1080/00268970412331319254.
(19) Luo, Y.; Ågren, H.; Vahtras, O.; Jørgensen, P. The Hyperpolarizability Dispersion of Para-Nitroaniline. *Chem. Phys. Lett.* **1993**, *207* (2–3), 190–194. https://doi.org/10.1016/0009-2614(93)87013-S.
(20) Norman, P.; Luo, Y.; Jonsson, D.; Ågren, H.; Sylvester-Hvid, K. O.; Mikkelsen, K. V. Hyperpolarizability Depolarization Ratios of Nitroanilines. *J. Chem. Phys.* **1997**, *107* (21), 9063–9066. https://doi.org/10.1063/1.475196.
(21) Norman, P.; Bishop, D. M.; Jensen, H. J. Aa.; Oddershede, J. Nonlinear Response Theory with Relaxation: The First-Order Hyperpolarizability. *J. Chem. Phys.* **2005**, *123* (19), 194103. https://doi.org/10.1063/1.2107627.
(22) Kaatz, P.; Donley, E. A.; Shelton, D. P. A Comparison of Molecular Hyperpolarizabilities from Gas and Liquid Phase Measurements. *J. Chem. Phys.* **1998**, *108* (3), 849–856. https://doi.org/10.1063/1.475448.
(23) Oudar, J. L.; Chemla, D. S. Hyperpolarizabilities of the Nitroanilines and Their Relations to the Excited State Dipole Moment. *J. Chem. Phys.* **1977**, *66* (6), 2664–2668. https://doi.org/10.1063/1.434213.

(24) Cheng, L. T.; Tam, W.; Stevenson, S. H.; Meredith, G. R.; Rikken, G.; Marder, S. R. Experimental Investigations of Organic Molecular Nonlinear Optical Polarizabilities. 1. Methods and Results on Benzene and Stilbene Derivatives. *J. Phys. Chem.* **1991**, *95* (26), 10631–10643. https://doi.org/10.1021/j100179a026.
(25) Oudar, J. L. Optical Nonlinearities of Conjugated Molecules. Stilbene Derivatives and Highly Polar Aromatic Compounds. *J. Chem. Phys.* **1977**, *67* (2), 446–457. https://doi.org/10.1063/1.434888.
(26) de Wergifosse, M.; Champagne, B. Electron Correlation Effects on the First Hyperpolarizability of Push–Pull π-Conjugated Systems. *J. Chem. Phys.* **2011**, *134* (7), 074113. https://doi.org/10.1063/1.3549814.
(27) Marder, S. R.; Beratan, D. N.; Cheng, L.-T. Approaches for Optimizing the First Electronic Hyperpolarizability of Conjugated Organic Molecules. *Science* **1991**, *252* (5002), 103–106. https://doi.org/10.1126/science.252.5002.103.
(28) Berkovic, G.; Meshulam, G.; Kotler, Z. Measurement and Analysis of Molecular Hyperpolarizability in the Two-Photon Resonance Regime. *J. Chem. Phys.* **2000**, *112* (9), 3997–4003. https://doi.org/10.1063/1.480991.
(29) Takimoto, Y.; Isborn, C. M.; Eichinger, B. E.; Rehr, J. J.; Robinson, B. H. Frequency and Solvent Dependence of Nonlinear Optical Properties of Molecules. *J. Phys. Chem. C* **2008**, *112* (21), 8016–8021. https://doi.org/10.1021/jp800444j.
(30) O'Neill, D. P.; Kállay, M.; Gauss, J. Calculation of Frequency-Dependent Hyperpolarizabilities Using General Coupled-Cluster Models. *J. Chem. Phys.* **2007**, *127* (13), 134109. https://doi.org/10.1063/1.2770714.
(31) Karna, S. P.; Prasad, P. N.; Dupuis, M. Nonlinear Optical Properties of *p* -nitroaniline: An *Ab Initio* Time-dependent Coupled Perturbed Hartree–Fock Study. *J. Chem. Phys.* **1991**, *94* (2), 1171–1181. https://doi.org/10.1063/1.460024.
(32) Burland, D. M.; Kajzar, F.; Sentein, C.; Walsh, C. A. Comparison of Hyperpolarizabilities Obtained with Different Experimental Methods and Theoretical Techniques. *J. Opt. Soc. Am. B* **1991**, *8* (11), 2269. https://doi.org/10.1364/JOSAB.8.002269.
(33) Suponitsky, K. Yu.; Tafur, S.; Masunov, A. E. Applicability of Hybrid Density Functional Theory Methods to Calculation of Molecular Hyperpolarizability. *J. Chem. Phys.* **2008**, *129* (4), 044109. https://doi.org/10.1063/1.2936121.
(34) Day, P. N.; Pachter, R.; Nguyen, K. A. Analysis of Nonlinear Optical Properties in Donor–Acceptor Materials. *J. Chem. Phys.* **2014**, *140* (18), 184308. https://doi.org/10.1063/1.4874267.
(35) Hammond, J. R.; Kowalski, K. Parallel Computation of Coupled-Cluster Hyperpolarizabilities. *J. Chem. Phys.* **2009**, *130* (19), 194108. https://doi.org/10.1063/1.3134744.
(36) Champagne, B.; Perpète, E. A.; Jacquemin, D.; van Gisbergen, S. J. A.; Baerends, E.-J.; Soubra-Ghaoui, C.; Robins, K. A.; Kirtman, B. Assessment of Conventional Density Functional Schemes for Computing the Dipole Moment and (Hyper)Polarizabilities of Push−Pull π-Conjugated Systems. *J. Phys. Chem. A* **2000**, *104* (20), 4755–4763. https://doi.org/10.1021/jp993839d.
(37) Dreuw, A.; Head-Gordon, M. Failure of Time-Dependent Density Functional Theory for Long-Range Charge-Transfer Excited States: The Zincbacteriochlorin−Bacteriochlorin and Bacteriochlorophyll−Spheroidene Complexes. *J. Am. Chem. Soc.* **2004**, *126* (12), 4007–4016. https://doi.org/10.1021/ja039556n.

(38) Dreuw, A.; Weisman, J. L.; Head-Gordon, M. Long-Range Charge-Transfer Excited States in Time-Dependent Density Functional Theory Require Non-Local Exchange. *J. Chem. Phys.* **2003**, *119* (6), 2943–2946. https://doi.org/10.1063/1.1590951.
(39) Iikura, H.; Tsuneda, T.; Yanai, T.; Hirao, K. A Long-Range Correction Scheme for Generalized-Gradient-Approximation Exchange Functionals. *J. Chem. Phys.* **2001**, *115* (8), 3540–3544. https://doi.org/10.1063/1.1383587.
(40) Tawada, Y.; Tsuneda, T.; Yanagisawa, S.; Yanai, T.; Hirao, K. A Long-Range-Corrected Time-Dependent Density Functional Theory. *J. Chem. Phys.* **2004**, *120* (18), 8425–8433. https://doi.org/10.1063/1.1688752.
(41) Vydrov, O. A.; Scuseria, G. E. Assessment of a Long-Range Corrected Hybrid Functional. *J. Chem. Phys.* **2006**, *125* (23), 234109. https://doi.org/10.1063/1.2409292.
(42) Toulouse, J.; Colonna, F.; Savin, A. Long-Range--Short-Range Separation of the Electron-Electron Interaction in Density-Functional Theory. *Phys. Rev. A* **2004**, *70* (6), 062505. https://doi.org/10.1103/PhysRevA.70.062505.
(43) Kirtman, B.; Bonness, S.; Ramirez-Solis, A.; Champagne, B.; Matsumoto, H.; Sekino, H. Calculation of Electric Dipole (Hyper)Polarizabilities by Long-Range-Correction Scheme in Density Functional Theory: A Systematic Assessment for Polydiacetylene and Polybutatriene Oligomers. *J. Chem. Phys.* **2008**, *128* (11), 114108. https://doi.org/10.1063/1.2885051.
(44) Sekino, H.; Maeda, Y.; Kamiya, M.; Hirao, K. Polarizability and Second Hyperpolarizability Evaluation of Long Molecules by the Density Functional Theory with Long-Range Correction. *J. Chem. Phys.* **2007**, *126* (1), 014107. https://doi.org/10.1063/1.2428291.
(45) Autschbach, J.; Srebro, M. Delocalization Error and "Functional Tuning" in Kohn–Sham Calculations of Molecular Properties. *Acc. Chem. Res.* **2014**, *47* (8), 2592–2602. https://doi.org/10.1021/ar500171t.
(46) Nénon, S.; Champagne, B.; Spassova, M. I. Assessing Long-Range Corrected Functionals with Physically-Adjusted Range-Separated Parameters for Calculating the Polarizability and the Second Hyperpolarizability of Polydiacetylene and Polybutatriene Chains. *Phys. Chem. Chem. Phys.* **2014**, *16* (15), 7083–7088. https://doi.org/10.1039/C4CP00105B.
(47) Stein, T.; Kronik, L.; Baer, R. Reliable Prediction of Charge Transfer Excitations in Molecular Complexes Using Time-Dependent Density Functional Theory. *J. Am. Chem. Soc.* **2009**, *131* (8), 2818–2820. https://doi.org/10.1021/ja8087482.
(48) Stein, T.; Kronik, L.; Baer, R. Prediction of Charge-Transfer Excitations in Coumarin-Based Dyes Using a Range-Separated Functional Tuned from First Principles. *J. Chem. Phys.* **2009**, *131* (24), 244119. https://doi.org/10.1063/1.3269029.
(49) Stein, T.; Eisenberg, H.; Kronik, L.; Baer, R. Fundamental Gaps in Finite Systems from Eigenvalues of a Generalized Kohn-Sham Method. *Phys. Rev. Lett.* **2010**, *105* (26), 266802. https://doi.org/10.1103/PhysRevLett.105.266802.
(50) Kronik, L.; Stein, T.; Refaely-Abramson, S.; Baer, R. Excitation Gaps of Finite-Sized Systems from Optimally Tuned Range-Separated Hybrid Functionals. *J. Chem. Theory Comput.* **2012**, *8* (5), 1515–1531. https://doi.org/10.1021/ct2009363.
(51) Koopmans, T. Über die Zuordnung von Wellenfunktionen und Eigenwerten zu den Einzelnen Elektronen Eines Atoms. *Physica* **1934**, *1* (1), 104–113. https://doi.org/10.1016/S0031-8914(34)90011-2.
(52) Sun, H.; Autschbach, J. Influence of the Delocalization Error and Applicability of Optimal Functional Tuning in Density Functional Calculations of Nonlinear Optical Properties of

Organic Donor–Acceptor Chromophores. *ChemPhysChem* **2013**, *14* (11), 2450–2461. https://doi.org/10.1002/cphc.201300256.
(53) Garrett, K.; Sosa Vazquez, X.; Egri, S. B.; Wilmer, J.; Johnson, L. E.; Robinson, B. H.; Isborn, C. M. Optimum Exchange for Calculation of Excitation Energies and Hyperpolarizabilities of Organic Electro-Optic Chromophores. *J. Chem. Theory Comput.* **2014**, *10* (9), 3821–3831. https://doi.org/10.1021/ct500528z.
(54) Ye, J.-T.; Liu, J.-H.; Zhang, Q.; Qiu, Y.-Q.; Wang, L.-H. Tuning of Second-Order Nonlinear Optical Properties Based on [2.2]Paracyclophanes Isomer: The Relative Configuration and Polarizable Environment. *J. Phys. Chem. C* **2020**, *124* (39), 21692–21701. https://doi.org/10.1021/acs.jpcc.0c05980.
(55) Frisch, M. J.; Trucks, G. W.; Schlegel, H. B.; Scuseria, G. E.; Robb, M. A.; Cheeseman, J. R. Gaussian 16, Revision C.01, 2016.
(56) Aidas, K.; Angeli, C.; Bak, K. L.; Bakken, V.; Bast, R.; Boman, L.; Christiansen, O.; Cimiraglia, R.; Coriani, S.; Dahle, P.; Dalskov, E. K.; Ekström, U.; Enevoldsen, T.; Eriksen, J. J.; Ettenhuber, P.; Fernández, B.; Ferrighi, L.; Fliegl, H.; Frediani, L.; Hald, K.; Halkier, A.; Hättig, C.; Heiberg, H.; Helgaker, T.; Hennum, A. C.; Hettema, H.; Hjertenæs, E.; Høst, S.; Høyvik, I.-M.; Iozzi, M. F.; Jansík, B.; Jensen, H. J. Aa.; Jonsson, D.; Jørgensen, P.; Kauczor, J.; Kirpekar, S.; Kjærgaard, T.; Klopper, W.; Knecht, S.; Kobayashi, R.; Koch, H.; Kongsted, J.; Krapp, A.; Kristensen, K.; Ligabue, A.; Lutnæs, O. B.; Melo, J. I.; Mikkelsen, K. V.; Myhre, R. H.; Neiss, C.; Nielsen, C. B.; Norman, P.; Olsen, J.; Olsen, J. M. H.; Osted, A.; Packer, M. J.; Pawlowski, F.; Pedersen, T. B.; Provasi, P. F.; Reine, S.; Rinkevicius, Z.; Ruden, T. A.; Ruud, K.; Rybkin, V. V.; Sałek, P.; Samson, C. C. M.; de Merás, A. S.; Saue, T.; Sauer, S. P. A.; Schimmelpfennig, B.; Sneskov, K.; Steindal, A. H.; Sylvester-Hvid, K. O.; Taylor, P. R.; Teale, A. M.; Tellgren, E. I.; Tew, D. P.; Thorvaldsen, A. J.; Thøgersen, L.; Vahtras, O.; Watson, M. A.; Wilson, D. J. D.; Ziolkowski, M.; Ågren, H. The Dalton Quantum Chemistry Program System. *WIREs Comput. Mol. Sci.* **2014**, *4* (3), 269–284. https://doi.org/10.1002/wcms.1172.
(57) Yanai, T.; Tew, D. P.; Handy, N. C. A New Hybrid Exchange–Correlation Functional Using the Coulomb-Attenuating Method (CAM-B3LYP). *Chem. Phys. Lett.* **2004**, *393* (1), 51–57. https://doi.org/10.1016/j.cplett.2004.06.011.
(58) Ditchfield, R.; Hehre, W. J.; Pople, J. A. Self-Consistent Molecular-Orbital Methods. IX. An Extended Gaussian-Type Basis for Molecular-Orbital Studies of Organic Molecules. *J. Chem. Phys.* **1971**, *54* (2), 724–728. https://doi.org/10.1063/1.1674902.
(59) Hehre, W. J.; Ditchfield, R.; Pople, J. A. Self—Consistent Molecular Orbital Methods. XII. Further Extensions of Gaussian—Type Basis Sets for Use in Molecular Orbital Studies of Organic Molecules. *J. Chem. Phys.* **1972**, *56* (5), 2257–2261. https://doi.org/10.1063/1.1677527.
(60) Hariharan, P. C.; Pople, J. A. The Influence of Polarization Functions on Molecular Orbital Hydrogenation Energies. *Theor. Chim. Acta* **1973**, *28* (3), 213–222. https://doi.org/10.1007/BF00533485.
(61) Rassolov, V. A.; Ratner, M. A.; Pople, J. A.; Redfern, P. C.; Curtiss, L. A. 6-31G* Basis Set for Third-Row Atoms. *J. Comput. Chem.* **2001**, *22* (9), 976–984. https://doi.org/10.1002/jcc.1058.
(62) Francl, M. M.; Pietro, W. J.; Hehre, W. J.; Binkley, J. S.; Gordon, M. S.; DeFrees, D. J.; Pople, J. A. Self-consistent Molecular Orbital Methods. XXIII. A Polarization-type Basis Set

for Second-row Elements. *J. Chem. Phys.* **1982**, *77* (7), 3654–3665. https://doi.org/10.1063/1.444267.
(63) Gordon, M. S.; Binkley, J. S.; Pople, J. A.; Pietro, W. J.; Hehre, W. J. Self-Consistent Molecular-Orbital Methods. 22. Small Split-Valence Basis Sets for Second-Row Elements. *J. Am. Chem. Soc.* **1982**, *104* (10), 2797–2803. https://doi.org/10.1021/ja00374a017.
(64) Becke, A. D. Density-functional Thermochemistry. III. The Role of Exact Exchange. *J. Chem. Phys.* **1993**, *98* (7), 5648–5652. https://doi.org/10.1063/1.464913.
(65) Chai, J.-D.; Head-Gordon, M. Long-Range Corrected Hybrid Density Functionals with Damped Atom–Atom Dispersion Corrections. *Phys. Chem. Chem. Phys.* **2008**, *10* (44), 6615–6620. https://doi.org/10.1039/B810189B.
(66) Chai, J.-D.; Head-Gordon, M. Systematic Optimization of Long-Range Corrected Hybrid Density Functionals. *J. Chem. Phys.* **2008**, *128* (8), 084106. https://doi.org/10.1063/1.2834918.
(67) Runge, E.; Gross, E. K. U. Density-Functional Theory for Time-Dependent Systems. *Phys. Rev. Lett.* **1984**, *52* (12), 997–1000. https://doi.org/10.1103/PhysRevLett.52.997.
(68) Tomasi, J.; Mennucci, B.; Cammi, R. Quantum Mechanical Continuum Solvation Models. *Chem. Rev.* **2005**, *105* (8), 2999–3094. https://doi.org/10.1021/cr9904009.
(69) Dunning, T. H. Gaussian Basis Sets for Use in Correlated Molecular Calculations. I. The Atoms Boron through Neon and Hydrogen. *J. Chem. Phys.* **1989**, *90* (2), 1007–1023. https://doi.org/10.1063/1.456153.
(70) Kendall, R. A.; Dunning, T. H.; Harrison, R. J. Electron Affinities of the First-row Atoms Revisited. Systematic Basis Sets and Wave Functions. *J. Chem. Phys.* **1992**, *96* (9), 6796–6806. https://doi.org/10.1063/1.462569.
(71) Kronik, L.; Kümmel, S. Dielectric Screening Meets Optimally Tuned Density Functionals. *Adv. Mater.* **2018**, *30* (41), 1706560. https://doi.org/10.1002/adma.201706560.
(72) Wang, C. H. Effects of Dephasing and Vibronic Structure on the First Hyperpolarizability of Strongly Charge-Transfer Molecules. *J. Chem. Phys.* **2000**, *112* (4), 1917–1924. https://doi.org/10.1063/1.480754.
(73) Orr, B. J.; Ward, J. F. Perturbation Theory of the Non-Linear Optical Polarization of an Isolated System. *Mol. Phys.* **1971**, *20* (3), 513–526. https://doi.org/10.1080/00268977100100481.
(74) Ward, J. F. Calculation of Nonlinear Optical Susceptibilities Using Diagrammatic Perturbation Theory. *Rev. Mod. Phys.* **1965**, *37* (1), 1–18. https://doi.org/10.1103/RevModPhys.37.1.
(75) Meshulam, G.; Berkovic, G.; Kotler, Z.; Sa'ar, A. Electric Field Induced Second Harmonic Generation with and without Fringes. *Rev. Sci. Instrum.* **2000**, *71* (9), 3490–3493. https://doi.org/10.1063/1.1287629.
(76) Hu, Z.; Autschbach, J.; Jensen, L. Simulating Third-Order Nonlinear Optical Properties Using Damped Cubic Response Theory within Time-Dependent Density Functional Theory. *J. Chem. Theory Comput.* **2016**, *12* (3), 1294–1304. https://doi.org/10.1021/acs.jctc.5b01060.
(77) Willetts, A.; Rice, J. E.; Burland, D. M.; Shelton, D. P. Problems in the Comparison of Theoretical and Experimental Hyperpolarizabilities. *J. Chem. Phys.* **1992**, *97* (10), 7590–7599. https://doi.org/10.1063/1.463479.
(78) Garza, A. J.; Wazzan, N. A.; Asiri, A. M.; Scuseria, G. E. Can Short- and Middle-Range Hybrids Describe the Hyperpolarizabilities of Long-Range Charge-Transfer Compounds? *J. Phys. Chem. A* **2014**, *118* (50), 11787–11796. https://doi.org/10.1021/jp510062b.

(79) Matsuzawa, N.; Dixon, D. A. Semiempirical Calculations of Hyperpolarizabilities for Donor-Acceptor Molecules: Comparison to Experiment. *J. Phys. Chem.* **1992**, *96* (15), 6232–6241. https://doi.org/10.1021/j100194a027.
(80) Quinet, O.; Kirtman, B.; Champagne, B. Analytical Time-Dependent Hartree-Fock Evaluation of the Dynamic Zero-Point Vibrationally Averaged (ZPVA) First Hyperpolarizability. *J. Chem. Phys.* **2003**, *118* (2), 505–513. https://doi.org/10.1063/1.1523903.
(81) Boyd, R. W. *Nonlinear Optics*; Academic press, 2020.
(82) Audebert, P.; Kamada, K.; Matsunaga, K.; Ohta, K. The Third-Order NLO Properties of D-π-A Molecules with Changing a Primary Amino Group into Pyrrole. *Chem. Phys. Lett.* **2003**, *367* (1), 62–71. https://doi.org/10.1016/S0009-2614(02)01575-0.
(83) Hu, Z.; Autschbach, J.; Jensen, L. Simulation of Resonance Hyper-Rayleigh Scattering of Molecules and Metal Clusters Using a Time-Dependent Density Functional Theory Approach. *J. Chem. Phys.* **2014**, *141* (12), 124305. https://doi.org/10.1063/1.4895971.
(84) Woodford, J. N.; Wang, C. H.; Asato, A. E.; Liu, R. S. H. Hyper-Rayleigh Scattering of Azulenic Donor–Acceptor Molecules at 1064 and 1907 Nm. *J. Chem. Phys.* **1999**, *111* (10), 4621–4628. https://doi.org/10.1063/1.479223.
(85) Campo, J.; Wenseleers, W.; Goovaerts, E.; Szablewski, M.; Cross, G. H. Accurate Determination and Modeling of the Dispersion of the First Hyperpolarizability of an Efficient Zwitterionic Nonlinear Optical Chromophore by Tunable Wavelength Hyper-Rayleigh Scattering. *J. Phys. Chem. C* **2008**, *112* (1), 287–296. https://doi.org/10.1021/jp0758824.

TOC